Nonlinear THz spectroscopy and simulation of gated graphene

Journal of Physics Communications

PAPER

Nonlinear THz spectroscopy and simulation of gated graphene

G Gäumann[1], I Crassee[2,3], N Numan[4,5], M Tamagnone[6,7], J R Mosig[6], J-M Poumirol[8], J-P Wolf[2] and T Feurer[1]

[1] Institute of Applied Physics, University of Bern, CH-3012 Bern, Switzerland
[2] GAP-Biophotonics, University of Geneva, CH-1211 Geneva, Switzerland
[3] Laboratoire National des Champs Magnétiques Intenses, CNRS-UGA-UPS-INSA, 38042 Grenoble, France
[4] Nanoscience and Nanotechnology, University of South Africa, ZA-0003 Pretoria, South Africa
[5] Material Research Department, iThemba LABS, ZA-7129 Somerset West, South Africa
[6] Laboratory of Electromagnetics and Antennas, École Polytechnique Fédérale de Lausanne, CH-1015 Lausanne, Switzerland
[7] Harvard John A. Paulson School of Engineering and Applied Sciences, Harvard University, Cambridge, Massachusetts 02138, United States of America
[8] DQMP, University of Geneva, CH-1211 Geneva, Switzerland

E-mail: iris.crassee@unige.ch

Keywords: nonlinear THz spectroscopy, high terahertz (THz) fields, graphene layers

Supplementary material for this article is available online

OPEN ACCESS

RECEIVED
22 May 2018

REVISED
5 June 2018

ACCEPTED FOR PUBLICATION
14 June 2018

PUBLISHED
28 June 2018

Abstract

We studied the nonlinear optical properties of single layer graphene using high terahertz (THz) fields. With the use of a back gate and cooling down the sample to cryogenic temperatures we are able to spectrally probe the nonlinear THz properties of intrinsic to highly doped graphene. The carrier density strongly affects the nonlinear properties of graphene; in the low doping and high THz field regime, an increase of the transmission on the order of 4% is found in our experiments. At higher doping levels we observe a larger relative nonlinear response: the larger the doping in the single layer the larger the relative field induced increase in transmission becomes. In all experiments, the THz field is opposing the effect of the gate, but field effects are never larger than the doping effects. We use the thermodynamical model for a hot electron gas also used by Mics *et al* (2015 *Nat. Commun.* **6** 7655) to simulate our data and study the effects of doping on the nonlinear properties of single layer graphene. We find that the highest carrier temperatures are obtained in low doped graphene. The model shows a good qualitative agreement with our data for high doping levels. Nevertheless our results demonstrate the limitation of the model for low doping levels. Our results are a road map for further explorations for the control of nonlinear light–matter interaction and functionalization of graphene layers in active THz devices in which carrier temperature and saturable absorption play a role.

1. Introduction

The unique electronic and optical properties of graphene stem from its relativistic low energy band dispersion. Near the K and K' point, massless Dirac Fermions have a linear energy–momentum dependence with a constant Fermi velocity of $v_F \approx c/300$ (c is the speed of light), making graphene particularly interesting for electronics and active optical applications [1].

In intrinsic graphene, the bands are filled up to the neutrality (Dirac) point and thus interband transitions can occur at every frequency of the impinging light. The linear band dispersion gives rise to $DOS(\omega) \propto \omega$, and therefore the optical conductivity is constant and equal to the universal optical conductivity, $\sigma_0 = e^2/4\hbar$ [2–4]. In doped graphene however, the bands are depleted below (hole doping) or filled above (electron doping) the Dirac point. Doped graphene exhibits distinct spectral regimes in which either intraband or interband transitions dominate the spectrum. In the low frequency regime, at terahertz (THz) frequencies, a Drude response is observed stemming from intraband transitions near the Fermi level. At higher frequency, but below the threshold of twice the chemical potential, optical transitions are blocked due to the Pauli principle resulting

in low conductivity. An onset of conductivity is centered around the value of twice the chemical potential, which is the frequency regime where interband transitions start to contribute to the optical response, above which the conductivity is reaching σ_0 [2]. Numerous optical studies have investigated the linear optical properties in the THz and infrared regime [5–7], showing clear doping controlled THz absorption.

Recent progress in THz graphene research has shown that even at modest fields on the order of tens of kV/cm a field dependent increase in transmission can be observed due to a nonlinear response of the excited carriers [8, 9–14]. With high field THz setups and high mobility large-area graphene samples more commonly available, the study of nonlinear THz properties has intensified significantly. The study of the field dependent optical properties has the potential to elucidate the fundamental processes leading to the observed saturable absorption, to test theoretical predictions of efficient higher harmonic generation [15–17], and to apply these promising unique spectral properties of graphene in high speed active optical devices.

In several recent works, the nonlinear optical properties of graphene have been modeled and explained using a thermodynamical model for a hot electron gas [8, 18, 19]. In [8] the heating dynamics of moderately doped single layer graphene at room temperature is reported and reproduced remarkably well. In this simple model, the carrier temperature in graphene is raised due to the absorption of the THz radiation and subsequent conversion into thermal energy. The increase of electronic temperature leads to the broadening of the Fermi–Dirac distribution and an associated lowering of the chemical potential. The shifts in electron temperature, chemical potential and possible decrease in scattering time together lead to saturable absorption.

The exceptional conductive properties of graphene drive the search for novel applications. However previous experiments and the results presented here show that intense THz fields compromise the conductivity of graphene, unfavorable for ultrafast high field THz graphene transistors [20–22]. For those applications it is pivotal to understand and avoid the reduction in conductivity. On the contrary, applications like THz detectors [23, 24] rely on the extraction of high-energy electrons. In this case a high electronic temperature is more critical than the associated reduction in conductivity. The nonlinear optical response of the carriers and therefore the field dependent reduction of the conductivity and the electronic temperature of the charge carriers, is dependent on the absorption of the THz light by those carriers. As the optical absorption is varying with the carrier density in the graphene sheet, the nonlinear THz response of graphene is expected to be strongly doping dependent [25]. The thermodynamical model used by Mics *et al* provides guidelines on how to increase the efficiency of graphene devices relying on the extraction of high-energy electrons; a higher electron temperature is beneficial, therefore graphene should be low doped such that the THz beam only heats a small number of carriers, heating them to extremely high temperatures [8]. On the contrary, their work predicts that the THz field driven reduction in conductivity is smallest in highly doped graphene.

Spurred on by the predictions of the hot electron gas model, we investigate experimentally the doping dependence of the nonlinear THz response and compare the results with simulations closely following the thermodynamical model. High field THz transmission experiments are performed on back-gated single layer CVD graphene. At low THz fields, we observe the expected doping dependent absorption. Next, we compare the THz response at neutral, low and high doping regimes for various THz field-strengths. Our results show that saturated absorption increases with doping. At moderate and high doping levels we find a reasonable match with the thermodynamical model, but for low doping the limitations of the model become significant. We explore different scattering mechanisms in the simulations and find that the energy dependence of the scattering plays a negligible role in the hot electron gas model.

2. Methods

The single layer graphene sample used in our optical study is a basic field-effect transistor, depicted schematically in figure 1(a). The Si/SiO_2 sample was fabricated from double sided polished high resistivity float zone silicon (thickness 525 μm, resistivity $>10000\ \Omega\cdot$cm) with 270 nm of thermally grown dry SiO_2. Gold contacts were defined on the Si wafer with dual layer lift-off resist (LOR) optical lithography, followed by e-beam evaporation (5 nm Cr followed by 50 nm Au) and lift-off; the wafer was subsequently diced. Large-area chemical-vapor deposited (CVD) monolayer graphene purchased from Graphenea S.A. was then transferred on the chip and on top of the metallic contacts. The monolayer measures about 5 by 5 mm, well above the THz diffraction limit. The metallic pads and the back side of the Si substrate are contacted with silver paint. With the back-gated device the doping of the graphene layer can be controlled and the resistance of the layer can be measured simultaneously. An example of a resistivity curve taken at 20 K is shown in figure 1(b). The curve clearly reveals the charge neutrality point at a gate voltage of about +40 V.

THz time-domain transmission spectra are measured at both 100 K and 200 K. A schematic representation of the experimental set-up is shown in figure 1(c). The graphene sample and a bare Si/SiO_2 substrate are both mounted in a vacuum chamber of a close cycle refrigerator in which the temperature of the sample and the

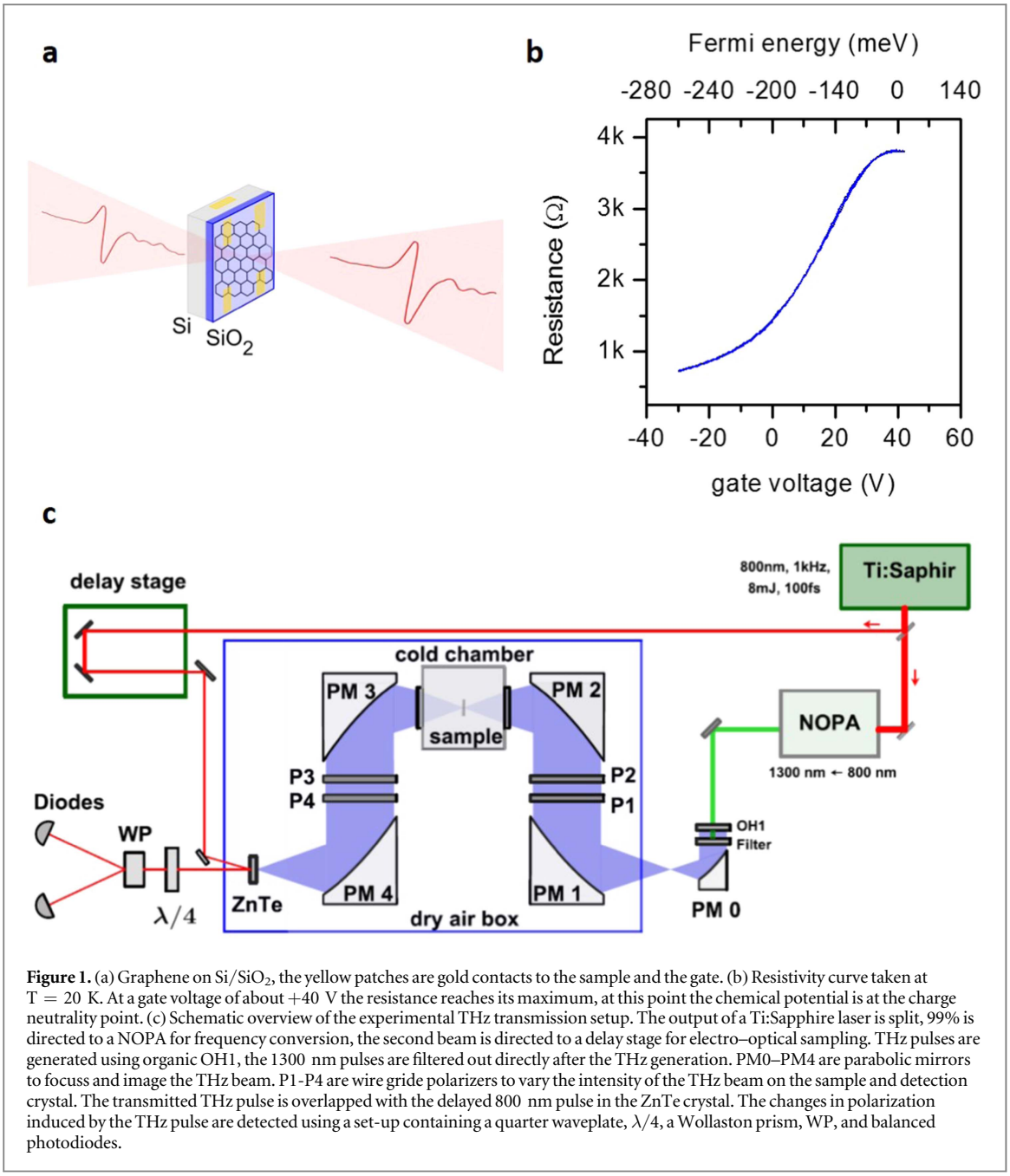

Figure 1. (a) Graphene on Si/SiO_2, the yellow patches are gold contacts to the sample and the gate. (b) Resistivity curve taken at $T = 20$ K. At a gate voltage of about +40 V the resistance reaches its maximum, at this point the chemical potential is at the charge neutrality point. (c) Schematic overview of the experimental THz transmission setup. The output of a Ti:Sapphire laser is split, 99% is directed to a NOPA for frequency conversion, the second beam is directed to a delay stage for electro–optical sampling. THz pulses are generated using organic OH1, the 1300 nm pulses are filtered out directly after the THz generation. PM0–PM4 are parabolic mirrors to focuss and image the THz beam. P1-P4 are wire gride polarizers to vary the intensity of the THz beam on the sample and detection crystal. The transmitted THz pulse is overlapped with the delayed 800 nm pulse in the ZnTe crystal. The changes in polarization induced by the THz pulse are detected using a set-up containing a quarter waveplate, $\lambda/4$, a Wollaston prism, WP, and balanced photodiodes.

reference substrate can be varied from room temperature down to 20 K. THz pulses are produced in an organic OH1 crystal pumped with 1300 nm infrared pulses coming from a NOPA. The resulting THz spectrum ranges from 0.1 to 2 THz and has a central frequency of 0.7 THz. The field strength is about 170 kV/cm, details of the calibration are given in the (see supplementary materials available online at stacks.iop.org/JPCO/2/065016/mmedia). The THz light path is dry air purged to avoid absorption by water vapor. Before impinging on the sample, the beam is collimated and the field strength is adjusted with the use of two THz polarizers, while the polarization direction is maintained. A second set of polarizers further reduces the THz field-strength, guaranteeing linear detection, and maintains the polarization direction of the light at the ZnTe detection crystal. The THz and 800 nm probe pulses propagate collinearly through the ZnTe crystal, the modulated polarization of the probe beam is measured using electro-optical sampling depicted in figure 1(c) [26]. The substrate or sample can be shifted in and out of the THz beam by moving the entire cold finger.

The simulation of the nonlinear THz response of graphene is based on the thermodynamical model proposed by Jensen *et al* [18] and Mics *et al* [8]. The carriers in graphene are therein described as a hot electron gas in thermal equilibrium. Upon excitation by an intense THz electric field, a finite amount of heat is added to the electron system and the electron temperature rises. The exchange of energy and momentum between those carriers in graphene is highly efficient due to the linear energy-momentum relation and takes place via elastic electron-electron interactions. Thermal equilibrium is reached at ~20 to 100 fs after excitation [18, 27–32],

while the electric field of the THz pulse oscillates on timescales of about 1ps. We assume that during interaction with the picosecond THz pulse the electron gas is continuously thermalized at elevated temperature T. The increase of the carrier temperature leads to the broadening of the Fermi–Dirac distribution and an associated lowering of the chemical potential. The field driven transmission increase is a direct consequence of the lowered chemical potential.

At time t_0, before the THz pulse arrives at the sample, the electron gas is fully characterized by the initial chemical potential $\mu_0 = \mu(t_0)$ and temperature $T_0 = T(t_0)$. The carriers are thermalized and can be described by the Fermi–Dirac distribution, $f_{FD}(\mu, T, E)$. The initial charge carrier concentration N_0 and thermal energy Q_0 of the electron gas are calculated using equations

$$N_0 = \int_0^\infty D(E) f_{FD}(\mu_0, T_0, E)\, dE \tag{1}$$

$$Q_0 = \int_0^\infty ED(E) f_{FD}(\mu_0, T_0, E)\, dE, \tag{2}$$

where $D(E)$ is the energy-dependent density of states and the zero point energy is set to the Dirac point. The maximal energies of the charge carriers is small enough to allow the use of the linearized expression of the density of states $D(E) = \frac{2}{\pi\hbar^2 v_F^2}|E|$, where $\hbar$ is the reduced Planck constant and we use $v_F = 1.0 \times 10^6$ m/s.

In CVD grown graphene, the chemical potential in graphene is often shifted far—tens to hundreds of meVs—from the Dirac point. The THz response of graphene, within a time step, is therefore completely dominated by free carrier intra-band transitions and thus Drude-like [2]. The resulting frequency dependent intra-band conductivity of a thermalized electron gas can be expressed as

$$\sigma(\omega) = -\frac{e^2 v_F^2}{2} \int_0^\infty D(E) \frac{\tau(E)}{1 - i\omega\tau(E)} \frac{\partial f_{FD}(\mu, T, E)}{\partial E} dE, \tag{3}$$

where e is the elementary charge and $\tau(E)$ is the energy dependent electron scattering time. With the use of the thin film equation [33] the absorption of the graphene is calculated.

With the simulated absorption, $A(t_0)$, of the graphene layer and the incoming THz field for the next time step $E_{THz}(t_1)$, the added thermal energy $\Delta Q(t_1)$ is determined. If all absorbed energy contributes to the electron gas heating, the added thermal energy is

$$\Delta Q(t) = c\varepsilon_0 \int_0^\infty R(t') A(t - t') E_{THz}(t - t')^2 dt' \tag{4}$$

where ε_0 is the vacuum permittivity and $R(t)$ describes the dissipation of heat by the carriers, described in the supplementary materials. The thermal energy balance equations reads:

$$Q_0 + \Delta Q(t_1) = Q_1 = \int_0^\infty ED(E) f_{FD}(\mu_1, T_1, E)\, dE. \tag{5}$$

Equation (5) and the conservation of carrier concentration:

$$N_0 = N(t_1) = N_1 = \int_0^\infty D(E) f_{FD}(\mu_1, T_1, E)\, dE \tag{6}$$

dictate the chemical potential, $\mu(t_0 + \Delta t) = \mu_1$, and temperature for the next time step, $T(t_0 + \Delta t) = T_1$, of the electron gas, which are inevitably changed.

The entire THz pulse, see figure 2(a), is propagated through the graphene layer in time steps of $\Delta t = 15$ fs. For each Δt, equations (1)–(4) are applied in combination with equations (5) and (6), resulting in a time-dependent carrier temperature, chemical potential, effective scattering time and thus in time-dependent optical properties.

Figure 2(b) shows the temporal evolution of the electron gas thermal energy. While the absorption of a THz pulse cumulatively increases the thermal energy Q, phonon assisted dissipation leads Q to return to the initial value Q_0 within hundreds of femtoseconds. Our simulations show that a larger initial chemical potential results in the highest absolute thermal energy. But the relative increase of the thermal energy is largest for low doped graphene: Q shows a ~8 fold increase for $\mu = 100$ meV and a four fold increase for $\mu = 220$ meV, when the field strength (FS) = 170 kV/cm. Figure 2(c) illustrates the carrier temperature behavior during the interaction. Clearly, highest carrier temperatures are observed for the smaller initial carrier concentrations. This result can be intuitively understood as the same energy Q is shared by fewer carriers resulting in a higher carrier temperature. The reduction of the electron chemical potential, dictated by the conservation of electrons is shown in figure 2(d).

Here we consider both charge carrier types, namely electrons in the conduction band and holes in the valence band. On the ultrafast time scales of $15 \sim 20$ fs, the electron and hole distributions are described by separate shifts of the chemical potentials: $\mu_e = \mu_0 - \mu_1$ and $\mu_h = \mu_0 + \mu_1'$ and distinct elevated temperatures T_e and T_h so that both the electron and hole concentration separately are conserved. Figure 3 illustrates this

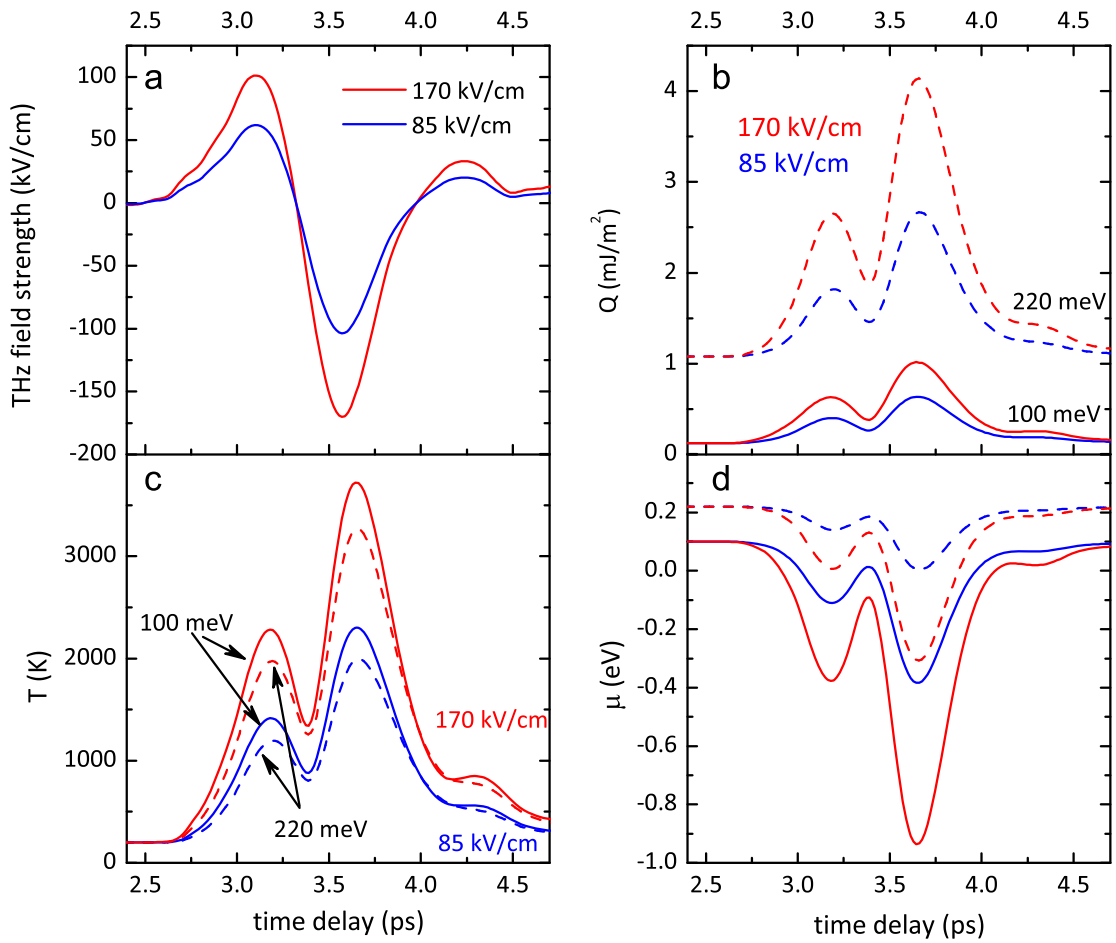

Figure 2. (a) Simulation of a THz pulse propagating through an electron doped single layer of graphene. The peak electric field-strengths are 85 and 170 kV/cm, the initial chemical potential of the modeled graphene is 220 meV at 200 K. The asymmetric shape of the pulse is a result of the pulse generation and not to interaction with graphene. Note also that the initial time at which the pulse starts, in this case 2.5 ps, is arbitrary. (b) The temporal evolution of thermal energy, for model graphene excited by a THz pulse with an 85 and 170 kV/cm field-strength and with $\mu = 100$ and 220 meV. (c) The temporal evolution of the carrier temperature, for the four corresponding cases in (b). (d) The temporal evolution of the chemical potentials, for the four corresponding cases in (b).

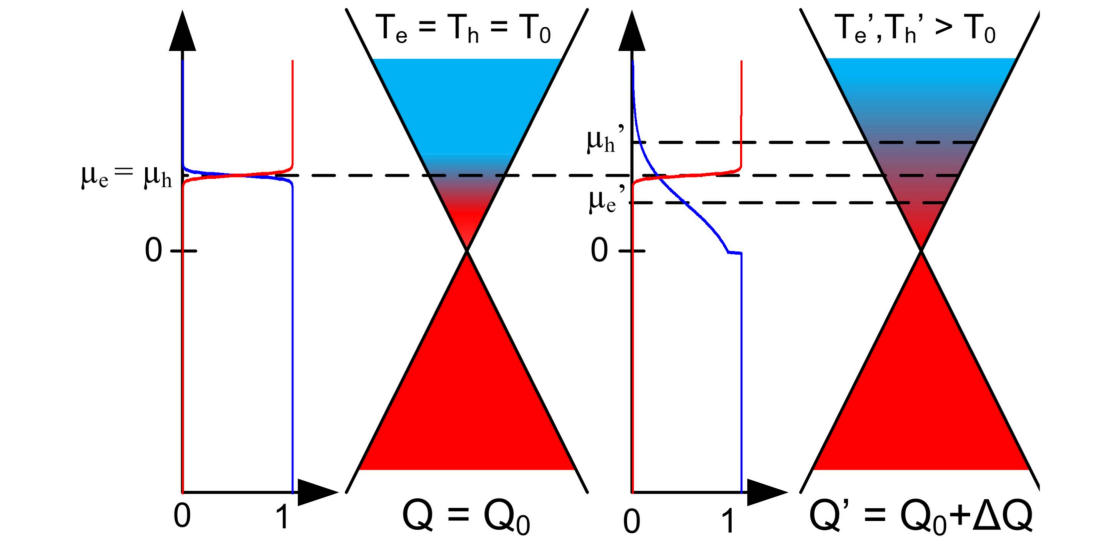

Figure 3. The incoming THz field adds some amount of thermal energy ΔQ to the carrier system which leads to an increase in the electron and hole temperature and a smear out of the Fermi–Dirac distributions. Without a change in the chemical potentials this would lead to an increase in concentration of both carrier types. Consequently the chemical potential of the electrons (holes) has to decrease (increase). Notice that the edge in the smeared out electron distribution occurs because only electrons in the conduction band (and holes in the valence band) are taken into account.

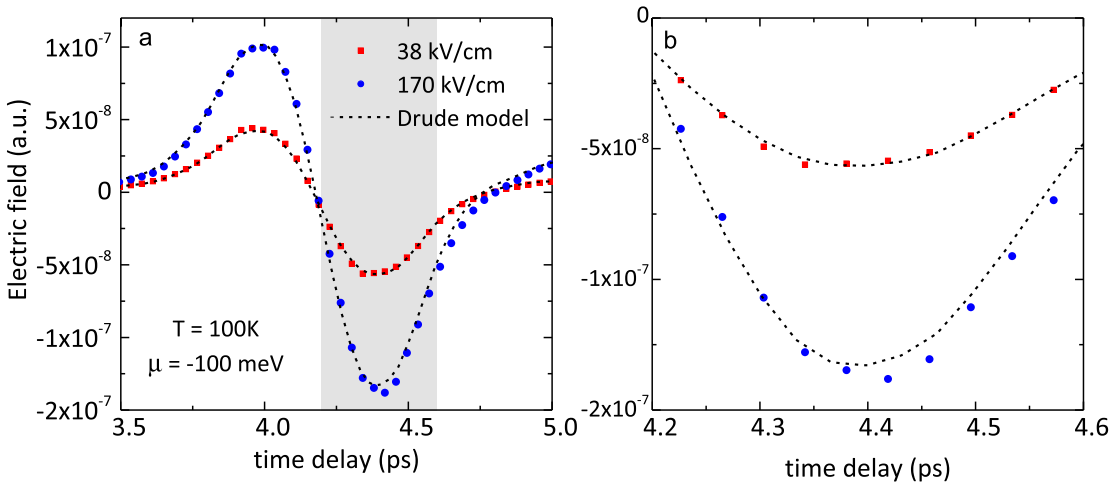

Figure 4. (a) Low THz field transmission analyzed using the Drude model. (b) A close-up of the main pulse of the THz time-domain spectra. The symbols show experimental data, the dashed lines are fits using the Drude model.

mechanism. Due to the independent conservation of electrons and holes, an initially electron doped graphene layer will retain its electron doping throughout the interaction with the THz pulse regardless of the shift in chemical potential.

The energy dependence of the scattering time, which varies for different scattering mechanisms, serves as an input parameter for the extraction of the optical conductivity of graphene using equation (3). In a first approach, we follow [8] and use a scattering time proportional to energy, $\tau(E) = \gamma E$ as is the case when long range scattering on Coulomb impurities dominates. An experimental estimate of γ is obtained from fitting the low field time-domain spectra and extracting $\tau(E_F)$ at E_F, then we use: $\gamma = \tau(E_F)/E_F$. In section 4.1, we compare different scattering regimes: energy independent, short- and long-range scattering and a combination as was reported for CVD graphene [34].

Note that field-strength, chemical potential, temperature, energy-dependent scattering time and density of states form a complete set of input parameters for the thermodynamical model and thus the model contains no free parameters.

For the simulations we strive to stay as close as possible to the thermodynamical model described in [8]. Thus, like is done in their work, we restrict the modeling to the contributions of electrons to the nonlinear optical properties and disregard the negligible contribution of hole-like carriers. Though our sample is in fact hole doped, due to electron-hole symmetry the contributions of electron-like and hole-like carriers are indistinguishable.

3. Low THz field response

In the limit of low THz fields the spectral response is field independent and therefore the time-domain spectra can be modeled using a simple linear Drude model taking into account the intra-band response observed in the THz regime [5, 13, 35]. The low THz field spectra are analysed using the Drude model, $\sigma(\omega) = \sigma_{DC}/(1 - i\omega\tau)$, where $\sigma_{DC} = D\tau/\pi$, ω is the frequency, D is the Drude weight and τ is the carrier scattering time, details are included in the supplementary materials. Figure 4(a) shows examples of Drude fits of experimental time-domain spectra at low and high THz fields. The Drude model shows very good agreement with the low field THz data. We observe a near perfect match between the optical Drude weight obtained from the analysis of the time-domain spectra and the weight calculated using E_F, obtained from transport measurements, connected through the relation $\hbar D/\sigma_0 = 2|E_F|$. The good match between optical spectral weight and Fermi energy indicate a good homogeneity and quality of the monolayer graphene probed by the entire THz spot. The carrier scattering extracted from the Drude analysis shows no significant dependence on the carrier concentration and is roughly 10 meV, which corresponds to a scattering time at the Fermi energy of $\tau(\varepsilon_F) \sim 400$ fs. We note however that the extraction of the Drude scattering in such a limited THz frequency range might prove unreliable.

Figure 4(b), a close-up of the main pulse, shows a discrepancy at high THz fields between the Drude model and the experimental data. The first half of the high field THz pulse evokes a transmission increase in the graphene. Therefore the experimental time-domain curve evidences a larger transmitted electric field in the second half of the THz pulse as opposed to the simulated transmission based on the Drude model (dashed line), demonstrating the limitations of this linear model.

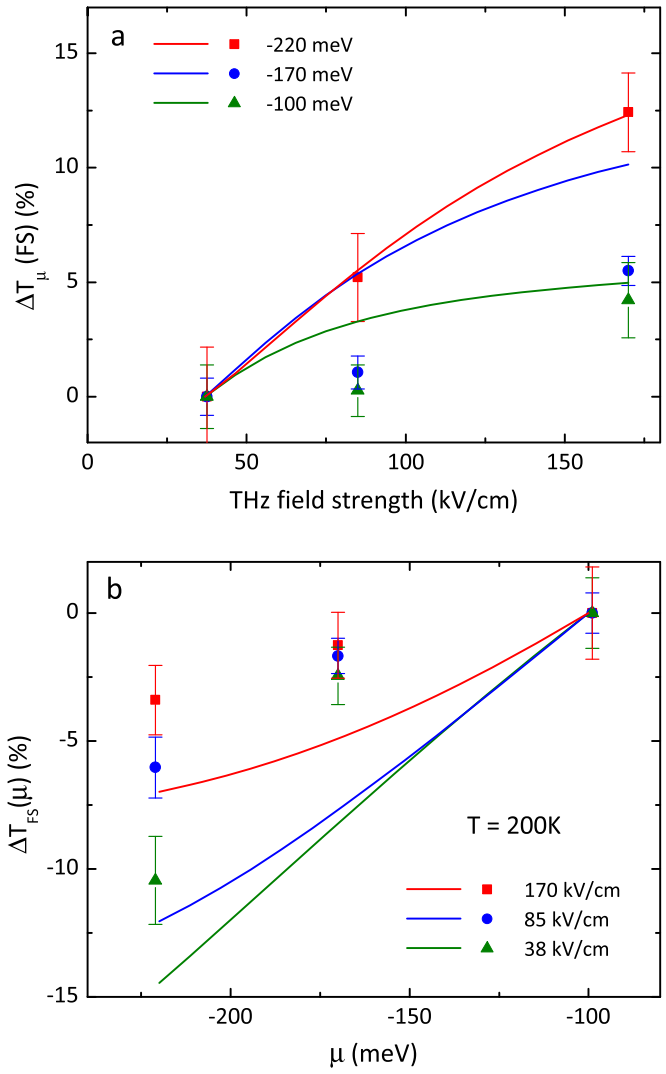

Figure 5. Normalized transmission as a function of chemical potential and THz field. The symbols show experimental data, the lines are obtained from the thermodynamical model. (a) The transmission normalized to the lowest THz field-strength at T = 200 K, as a function of THz field. (b) The transmission normalized to the lowest carrier concentration at T = 200 K, as a function of chemical potential for three different THz field-strengths.

4. High THz field response

The high THz field experimental and simulated time-domain spectra were measured and modeled using THz fields with a peak electric field up to 170 kV/cm, several carrier concentrations, at a temperature of 200 K. The peak-to-peak field-strength of a time-domain THz pulse, transmitted through the sample, represents an easy to extract but frequency averaged parameter, that allows to compare different measurements with each other. The sample peak-to-peak electric field ΔE_{gra} is normalized to the peak-to-peak electric field of the pristine (reference) pulse ΔE_{ref} for each THz field. This results in a value $dT(\mu, \mathrm{FS}) = \Delta E_{gra}(\mu, \mathrm{FS})/\Delta E_{ref}(\mathrm{FS})$, for each chemical potential and THz field-strength.

The thermalization of the electron gas takes place on a shorter time scale than the THz pulse duration. The total change in transmission, $dT(\mu, \mathrm{FS})$ extracted from the experimental data and the modeling, should not be interpreted as a nonlinear response to the maximal peak-to-peak electric field, but as an accumulation of the nonlinear response to fractions of the peak electric field.

Figure 5(a) shows the transmission normalized to the transmission at the lowest THz field-strength: $\Delta T_\mu(\mathrm{FS}) = (dT_\mu(\mathrm{FS}) - dT_\mu(\text{Low FS}))/dT_\mu(\text{Low FS})$. This normalization procedure is taken from [36] and improves the visibility of continuous changes. For a low chemical potential ($\mu = -100$ meV) a small relative increase in transmission, of about 4%, is observed when increasing the THz field, which is in agreement with previous studies. Importantly, upon increasing the chemical potential the increase in transmission becomes significantly larger(6% and 12.5%), showing that the relative saturable absorption is larger for a larger carrier concentration. We find the best agreement between model and experiment at the highest carrier concentration.

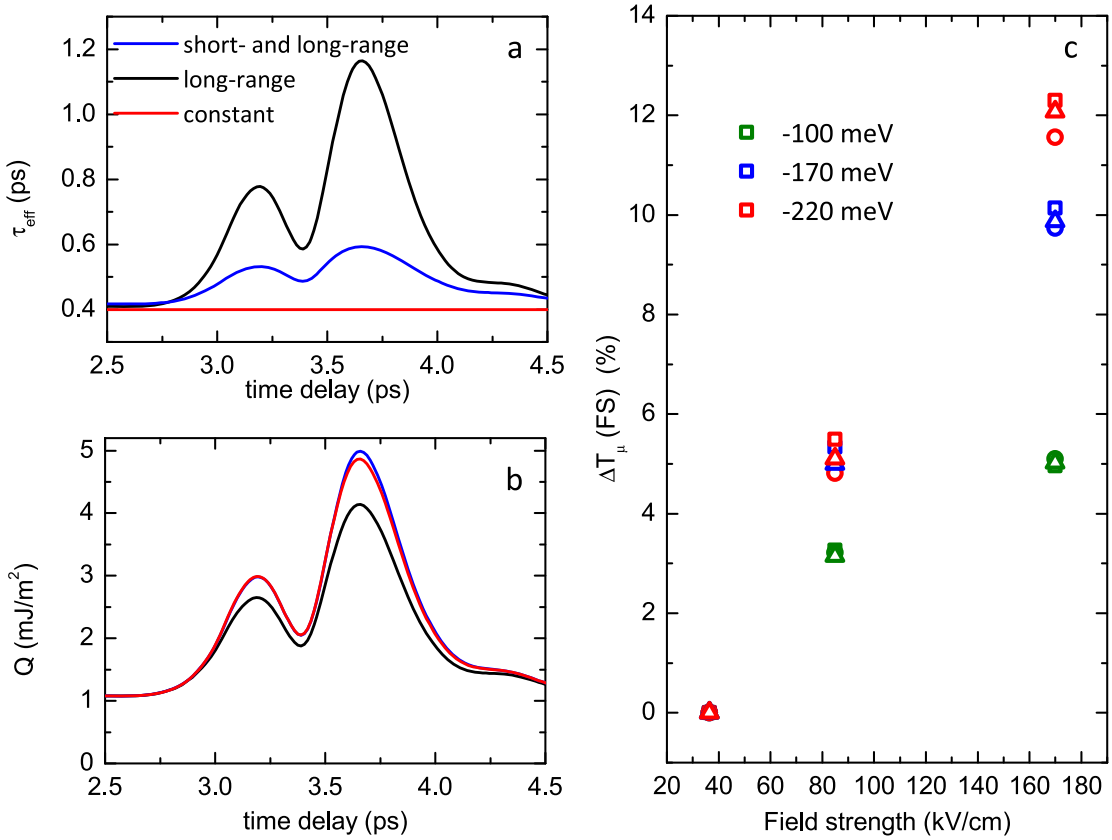

Figure 6. Temporal evolution of the effective scattering (a) and the thermal energy (b) for a field-strength of 170 kV/cm and an initial doping of 220 meV for different energy dependent scattering mechanisms. (c) THz field dependent relative transmission change for different doping. Colors indicate the initial doping of graphene. Symbols indicate long-range (squares), constant (circle) and short- and long-range (triangle) scattering.

The high relative nonlinear response at the highest doping level, does not contradict that for low carrier concentration the highest temperatures are expected. Due to the lower transmission at large carrier concentrations, relative changes are bigger. Note that simulations confirm that the lowest THz field of about 38 kV/cm is close enough to the linear regime in order to not have a major influence on the results.

Figure 5(b) shows the transmission normalized to the transmission at the lowest carrier concentration: $\Delta T_{FS}(\mu) = (dT_{FS}(\mu) - dT_{FS}(\text{Low } \mu))/dT_{FS}(\text{Low } \mu)$. One can clearly see that $\Delta T_{FS}(\mu)$ is reduced when the absolute value of the chemical potential is increased as it should be due to the increased Drude absorption by free carriers. While the maximum transmission decrease is $\Delta T \approx 11\%$ for low field-strength, it reduces to 3% for higher THz fields. The model and experimental data show qualitative agreement. Therefore the shifts in temperature and chemical potential driven by the absorption of the THz radiation indeed seem to be the origin of the observed saturable absorption. However, we note that the low field experimental data seems to match with intermediate and high field simulations. This discrepancy is due to the normalization to $dT_{FS}(\text{Low } \mu)$. The unsatisfactory match between model and data for low carrier concentration points out that the validity of the model is restricted to high doping levels where the optical response is completely determined by intraband transitions and the assumption that electron and hole concentrations are separately conserved is not too discordant. Thence, when normalized to low doping, the model is invalid and underestimates the effects of the THz field.

4.1. Scattering on Coulomb impurities and disorder

For CVD grown graphene previous work has assumed long-range scattering on Coulomb impurities to be the dominant scattering mechanism [36]. Coulomb scattering leads to a linearly increasing scattering time. A recent study found both long- and short-range (scattering on disorder) scattering in CVD graphene, such that $\tau(E) = \frac{|E|}{a + bE^2}$ [34, 37, 38]. We investigate different scattering regimes by substituting $\tau(E)$ in equation (3) by a constant energy independent scattering $\tau(E) = \tau(E_F)$, Coulomb scattering and lastly by a combination of short- and long-range scattering.

Figure 6(a) shows the temporal evolution of the effective scattering time, τ_{eff}, for each different scattering mechanisms. The effective scattering time is obtained by fitting the simulated conductivity using the Drude

model for every time step. A linear energy dependence of the scattering time on carrier energy leads to the biggest change in τ_{eff}. Figure 6(b) shows the influence of the scattering mechanism on the increase in thermal energy of the electron gas. The energy-independent scattering time leads to the highest absorbed energies, while a linear energy dependence keeps the thermal energy of the electrons lower. When both short- and long-range scattering are taken into account, the thermal energy of the electrons stays within the first two bounds.

In figure 6(c) the relative change in transmission, ΔT_{μ}(FS), for the three different scattering mechanisms is plotted for different initial doping. Clearly, the influence of $\tau(E)$ on the relative transmission changes $\Delta T(\mu, \mathrm{FS})$ is small. The proposed scattering mechanisms are thus indistinguishable based on our experimental data accuracy.

5. Conclusion

We have carried out THz spectroscopy measurements on single layer graphene for different THz field-strength and doping. At low THz fields the optical response of the graphene sample is accurately fitted using the Drude model with a Drude weight matching transport measurements, allowing to extract a scattering time of ~400 fs.

At higher THz fields, we see a gradual increase in the experimentally obtained relative transmission, which is also referred to as saturable absorption. This effect is doping dependent and shows the strongest relative changes at high carrier concentrations. Stronger THz fields therefore counteracts the effect of higher doping.

We compared our experimental results with the thermodynamical model for hot carriers. The model is in qualitative agreement with our data. Clearly the largest relative nonlinear response is observed for higher doped graphene, where the best match between model and data is found. However, it can not explain all our experimental data in a quantitative manner. In particular when the transmission is normalized to the lowest carrier concentration, the model underestimates the relative nonlinear effects.

We find that the relative nonlinear increase in transmission—or reduction in conductivity—is smallest for low doped graphene. Note that this is not in disagreement with previous reports, since we look at relative changes and not absolute values. This is supported by our simulations that show highest electron temperatures for low doping.

Different scattering mechanisms with individual energy dependencies, like long-range, constant or a combination of short- and long-range scattering are investigated, however our results obtained using the hot electron model illustrate the limited influence of the energy dependence of scattering on the relative transmission. We speculate that discrepancies observed between data and model might be due to limitations of the assumption that the electron gas is instantaneously thermalized. Alternatively, the properties of CVD graphene might play a role, as it exhibits grain boundaries and charge puddles.

Altogether we find that a THz induced increase in the electron temperature together with an associated shift of the chemical potential satisfyingly explain the saturable absorption observed in CVD graphene and we have shown that this nonlinear effect can be controlled by the initial Fermi energy with the use of a gate.

Acknowledgments

We thank Zoltán Mics and Dirk van der Marel for useful discussions. GG acknowledges funding from the Swiss National Science Foundation (SNSF) through project IZLSZ2_149164 and NCCR MUST. IC acknowledges funding from the NCCR MUST Inter-MUST Women Postdoc Award and MT acknowledges the SNSF grants 133583 and 168545.

ORCID iDs

I Crassee https://orcid.org/0000-0002-1288-9236

References

[1] Novoselov K S, Geim A K, Morozov S V, Jiang D, Dubonos S V, Grigorieva I V and Firsov A A 2004 *Science* **306** 666–9
[2] Ando T, Zheng Y and Suzuura H 2002 *J. Phys. Soc. Japan* **71** 1318–24
[3] Nair R R, Blake P, Grigorenko A N, Novoselov K S, Booth T J, Stauber T, Peres N M R and Geim A K 2008 *Science* **320** 1308
[4] Kuzmenko A B, van Heumen E, Carbone F and van der Marel D 2008 *Phys. Rev. Lett.* **100** 117401
[5] Mak K F, Sfeir M Y, Wu Y, Lui C H, Misewich J A and Heinz T F 2008 *Phys. Rev. Lett.* **101** 196405
[6] Horng J *et al* 2011 *Phys. Rev.* B **83** 165113
[7] Frenzel A J, Lui C H, Shin Y C, Kong J and Gedik N 2014 *Phys. Rev. Lett.* **113** 056602
[8] Mics Z, Tielrooij K J, Parvez K, Jensen S A, Ivanov I, Feng X, MÃllen K, Bonn M and Turchinovich D 2015 *Nat. Commun.* **6** 7655
[9] Frenzel A J, Lui C H, Fang W, Nair N L, Herring P K, Jarillo-Herrero P, Kong J and Gedik N 2013 *Appl. Phys. Lett.* **102** 113111

[10] Hwang H Y, Brandt N C, Farhat H, Hsu A L, Kong J and Nelson K A 2013 *The Journal of Physical Chemistry* B **117** 15819–24
[11] Paul M J *et al* 2013 *New J. Phys.* **15** 085019
[12] Paul M J, Lee B, Wardini J L, Thompson Z J, Stickel A D, Mousavian A, Choi H, Minot E D and Lee Y S 2014 *Appl. Phys. Lett.* **105** 221107
[13] Razavipour H *et al* 2015 *Phys. Rev.* B **92** 245421
[14] Choi H J *et al* 2017 *Sci. Rep.* **7** 42833
[15] Yoshikawa N, Tamaya T and Tanaka K 2017 *Science* **356** 736–8
[16] Mikhailov S A and Ziegler K 2008 *J. Phys.: Condens. Matter* **20** 384204
[17] Wright A R, Xu X G, Cao J C and Zhang C 2009 *Appl. Phys. Lett.* **95** 072101
[18] Jensen S A, Mics Z, Ivanov I, Varol H S, Turchinovich D, Koppens F H L, Bonn M and Tielrooij K J 2014 *Nano Lett.* **14** 5839–45
[19] Jadidi M M, König-Otto J C, Winnerl S, Sushkov A B, Drew H D, Murphy T E and Mittendorff M 2016 *Nano Lett.* **16** 2734–8
[20] Schwierz F 2010 *Nat. Nanotechnol.* **5** 487–96
[21] Wu Y, Lin Y M, Bol A A, Jenkins K A, Xia F, Farmer D B, Zhu Y and Avouris P 2011 *Nature* **472** 74–8
[22] Cheng R, Bai J, Liao L, Zhou H, Chen Y, Liu L, Lin Y C, Jiang S, Huang Y and Duan X 2012 *Proc. Natl Acad. Sci.* **109** 11588–92
[23] Mittendorff M, Winnerl S, Kamann J, Eroms J, Weiss D, Schneider H and Helm M 2013 *Appl. Phys. Lett.* **103** 021113
[24] Cai X, Sushkov A B, Suess R J, Jadidi M M, Jenkins G S, Nyakiti L O, Myers-Ward R L, Li S, Yan J, Gaskill D K, Murphy T E, Drew H D and Fuhrer M S 2014 *Nat. Nanotechnol.* **9** 814–9
[25] Shi S F, Tang T T, Zeng B, Ju L, Zhou Q, Zettl A and Wang F 2014 *Nano Lett.* **14** 1578–82
[26] Wu Q and Zhang X C 1995 *Appl. Phys. Lett.* **67** 3523–5
[27] Breusing M, Kuehn S, Winzer T, Malić E, Milde F, Severin N, Rabe J P, Ropers C, Knorr A and Elsaesser T 2011 *Phys. Rev.* B **83** 153410
[28] Tielrooij K J, Song J C W, Jensen S A, Centeno A, Pesquera A, Zurutuza Elorza A, Bonn M, Levitov L S and Koppens F H L 2013 *Nat. Phys.* **9** 248–52
[29] Gierz I, Petersen J C, Mitrano M, Cacho C, Turcu I C E, Springate E, Stohr A, kohler A, Starke U and Cavalleri A 2013 *Nat. Mater.* **12** 1119–24
[30] Johannsen J C *et al* 2013 *Phys. Rev. Lett.* **111** 027403
[31] Song J C W, Tielrooij K J, Koppens F H L and Levitov L S 2013 *Phys. Rev.* B **87** 155429
[32] Brida D, Tomadin A, Manzoni C, Kim Y J, Lombardo A, Milana S, Nair R R, Novoselov K S, Ferrari A C, Cerullo G and Polini M 2013 *Nat. Commun.* **4** 1987
[33] Glover R E and Tinkham M 1957 *Phys. Rev.* **108** 243–56
[34] Yu K, Kim J, Kim J Y, Lee W, Hwang J Y, Hwang E H and Choi E J 2016 *Phys. Rev.* B **94** 235404
[35] Kuzmenko A B 2005 *Rev. Sci. Instrum.* **76** 083108
[36] Hwang E and Das Sarma S 2008 *Phys. Rev.* B **77** 115449
[37] Hwang E H, Adam S and Sarma S D 2007 *Phys. Rev. Lett.* **98** 186806
[38] Das Sarma S, Adam S, Hwang E H and Rossi E 2011 *Rev. Mod. Phys.* **83** 407–70